Diffusion of proteins and determination of the friction coefficient of an amphiphilic bilayer

Joao Gomes
Wladimir Urbach

Laboratoire de Physique Statistique
de l'École Normale Supérieure de Paris, UMR CNRS 8550

April 5, 2007

Experimental Report, DEA of Theoretical Physics

Abstract

In Saffman's work on the brownian motion of cylindrical particles in biological membranes [7] is derived a logarithmic dependence of the diffusion coefficient on the radius of the particle. It was shown experimentally [8] that Saffman's solution no longer works for protein's mobility in liquid membranes. The experimental results suggest that the diffusion coefficient goes as the inverse of the radius. Starting from a Stokes-Einstein like equation for the diffusion coefficient, we try to determine the characteristic length, parameter introduced heuristically on the constant of proportionality between the diffusion coefficient and the inverse of the radius. It requires knowing both diffusion and friction's bilayer coefficients. We constructed and tested an experiment to determine the friction coefficient of an amphiphilic bilayer. Although we were able of determining the viscosity of some liquids with a good precision we couldn't determine the friction parameter.

Contents

1 Introduction

Bacteria can resist to antibiotics through a process known as efflux. This process functions via a dependent-energy mechanism (active transport) mediated by proteins which pump out the unwanted substances through the membrane. The required energy can be provided by transmembrane electrochemical gradient of protons (MFS, RND, SMR families) or sodium ions (MATE family) or by ATP hydrolysis (ABC family) [1]. The most frequently encountered pumps are of the RND-type such as AcrB in *Escherichia coli* or MexB in *Pseudomonas aeruginosa*. We are mainly interested in MexB pumps. This pump is constituted by three different proteins. OprM and MexB are, respectively, the outer and inner membrane proteins and MexA the membrane fusion protein (Fig.1).

Because of the helical structure of these proteins, they can be treated as cylindrical objects when studying diffusion processes. The hydrodynamic model of Saffman and Delbrück [7] for the problem of a diffusing cylinder in a thin sheet of fluid matching its height, predicts the following relation for the diffusion coefficient

$$D_{\text{Saffman}} = \frac{K_B T}{4\pi\mu_m h}\left(\ln\left(\frac{\mu_m h}{\mu_w R}\right) - \gamma\right),$$

where μ_m is the viscous coefficient of the membrane's liquid, μ_w is the viscosity of the surrounding liquid (typically water), h is the membrane's thickness, R is the radius of the protein and γ is the Euler constant. Because there isn't any analytical exact solution for the problem of the flow past a cylinder, Saffman's result constitutes a good approximation for the flow of a cylindrical object through an amphiphilic membrane taking into account the effect of the surrounding fluid. An experimental study of the mobility of proteins in membranes [8] showed that the dependence of the diffusion coefficient D on the radius R is stronger than the slow logarithmic dependence. The experimental data suggests that the coefficient D is inversely proportional to R and h. Y. Gambin *et al.* [8] proposed the expression

$$D = \frac{k_B T \lambda}{4\pi\mu_m h R},$$

where the characteristic length λ is introduced for dimensional reasons. They supposed that the membrane's viscosity was independent of h and its surface maintained flat over large distances. The values of the characteristic length can only be roughly estimated because of the difficulty in

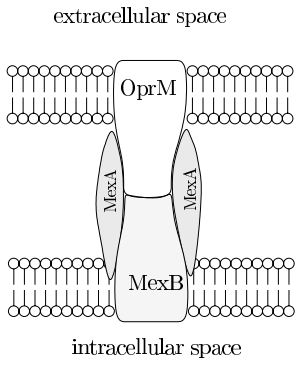

Figure 1: MexB RND-type pump.

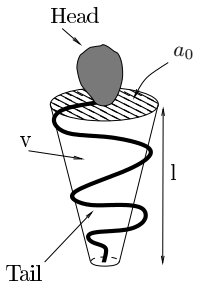

Figure 2: Representation of an amphiphilic molecule; a_0: area of the head group, v: volume of the molecule and l is its height.[3]

determining the bilayer's viscosity. It is supposed it can vary between 5 and 5000 Å. Although it is still too difficult to give it a meaning we think it can be related to the limits of validity of Saffman's hydrodynamic model. One can expect that in the limit $R \gg \lambda$ the Saffman's-Delbrück analysis still applies.

Our purpose is to determine the value of the characteristic length λ. To achieve it, our work will be made in two parts. The first consists in the construction of an experiment suitable to determine the membrane's viscosity μ_m and in the second we will use photobleaching techniques, namely the FRAPP (fluorescence recovery after photobleaching pattern), to determine the diffusion coefficient. We emphasize the fact that the FRAPP experience is straightforward work on the contrary to the viscosity which has never been done.

1.1 Amphiphilic structures

Surfactants are substances that can lower the surface tension of a liquid. They are usually organic compounds made of amphiphilic molecules. These molecules are composed of a hydrophobic group (tail) and a hydrophylic group (head) as shown in Fig.2. Their heads have affinity with water in contrast to the tails. The surfactants can be classified according to the polarity of the heads. They can be ionic or non-ionic if they are, respectively, charged or neutral, *zwitterionic* if they have the ability of acquiring charge or carrying electric dipoles or even amphoteric, i.e., they can be either ionic or non-ionic. Moreover, the molecule can acquire different shapes as a result of different factors like pH, temperature, concentration, composition, etc. As a result different packings can occur, from which different collective structures can be formed (Fig.3). They can be characterized by the parameter v/la_0, with v the volume of the molecule, l is its height and a_0 is the area of the head group. For conic structures or low v/la_0 spherical micelles (Fig.3a) are more probable to occur while for $v/la_0 \sim 1$ the lamellar ones are favored (Fig.3b). The transformation of one structure to another depends on different variables like temperature, the concentration of the species, the solvent, etc. More generally, it is achieved by an additive called co-surfactant. In other words, it means that if we fix the water and surfactant concentrations and add continuously co-surfactant we will see appearing sequentially those structures (Fig.4) .

The structure that interest us most is the lamellar one. In fact, as we will see, the viscosity's experiment is based on the flow of a lamellar phase liquid. As we see in Fig.3b they are composed of fine, alternating layers of amphiphilic molecules with a periodicity d. They are commonly

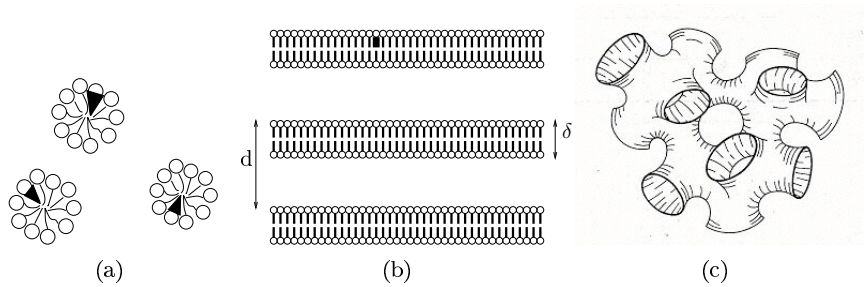

Figure 3: Different amphiphilic structures. a) spherical micelles (conic shape); b) lamellar phase or L_α (cilindrical shape); c) sponge phase or L_3.

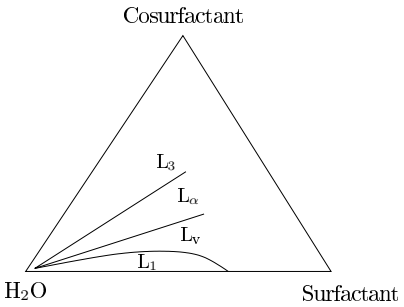

Figure 4: General phase diagram for an amphiphilic solution with water as solvent. Each vertex corresponds to 100% in volume. Typically these systems show the sequence: L_1(micelles)→L_v(vesicular phase)→L_α(lamellar phase)→L_3, when we add consecutively co-surfactant.[5]

characterized by the fraction

$$\phi = \frac{\delta}{d},$$

which corresponds to the volume fraction of the bilayer as we can easily verify. A commonly used system is composed of $H_2O \setminus C_{12}E_5 \setminus C_6E_0$[1]. Here C_6E_0, or hexanol, is the co-surfactant and $C_{12}E_5$ is a non-ionic surfactant composed of a six carbons long tail and a PEG head. They can form stable phases for a wide range of concentrations, which makes possible the study of different spaced structures (Fig.5).

[1]The $C_{12}E_5$ has the chemical formula: $H\text{-}(OCH_2H_2)_5OCH_2(CH_2)_{10}CH_3$

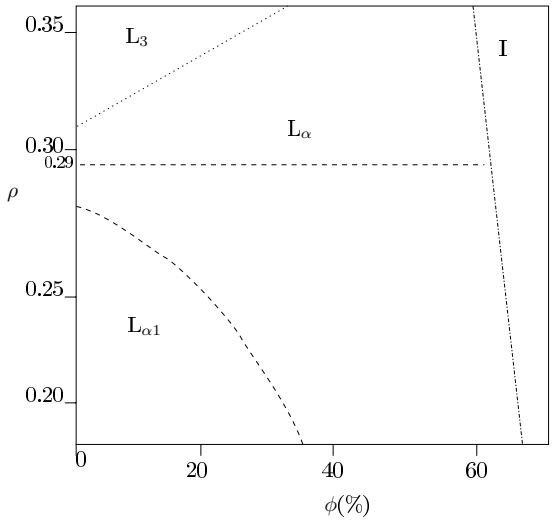

Figure 5: Phase diagram of the system $H_2O \setminus C_{12}E_5 \setminus C_6E_0$. The quantity ρ is the quotient between the mass of C_6E_0 and $C_{12}E_5$ for a temperature of 22°C. They are represented five different phases: lamellar phase (L_α); sponge phase (L_3); lamellar phase with diphasic micelles ($L_{\alpha 1}$); isotropic phase (I).(see [6]).

1.2 Couette flow due to gravity

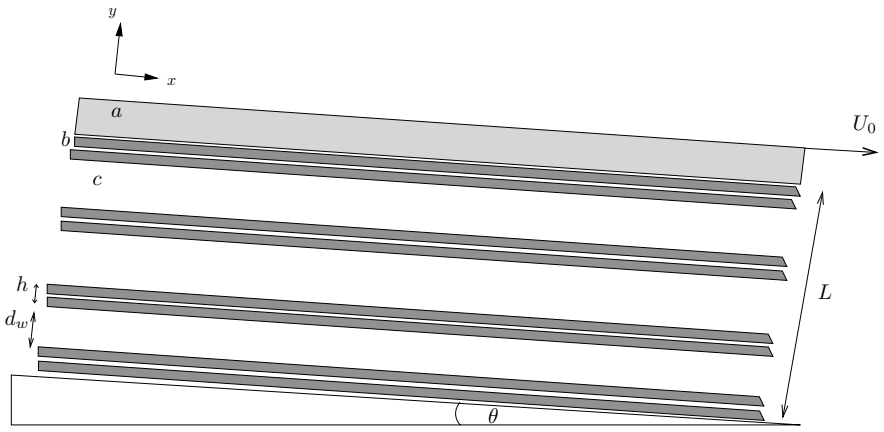

Figure 6: Shear cell with transversely oriented bilayers. a: lamelle of glass; b: amphiphilic bilayer; c: water layer;

To determine the membrane's shear viscosity we propose the idealized shear cell shown in Fig.6. The flow is due to the action of the gravity. In addition to the inertial movement of the fluid, there is also a stress f on the top of the flow due to the lamelle's weight. We consider N bilayers and $N-1$ water layers each of thickness $d_w = \frac{(L-Nh)}{N-1}$. We define Δu_n as the difference of velocity

between the two n^{th} amphiphilic layers and Δv_n as the difference of velocity between the faces of the n^{th} water layer (we count from the bottom). If we admit no slip boundary conditions we get

$$U_0 = \sum_{n=1}^{N} \Delta u_n + \sum_{n=1}^{N-1} \Delta v_n, \tag{1}$$

where U_0 is the velocity of the lamelle. Using the Navier-Stokes equations we determine the water flow pattern for the n^{th} layer

$$v(y) = -\frac{\rho_w}{2\eta_w} g y^2 \sin(\theta) + a_n y + v(0)$$

where ρ_w is the water density, η_w is the water viscosity ($8,90 \times 10^{-4}$Pa.s at $22°C$), g is the gravity's acceleration ($9,8$ m/s^2) and y is the transversal coordinate which goes from 0 to d_w. This way $v(0)$ is the velocity on the bottom of the water layer. To determine the constant a_n we use the relation

$$\tau = \eta_w \frac{\partial v}{\partial y},$$

where τ is the applied shear stress on the top of the water layer. As we can see from Fig.7 τ will be given by the stress f, due to the lamelle, plus the stress induced by the weight of $N-n-1$ water layers and $N-n$ bilayers which stand above,

$$\tau_n = f + (N-n)(\rho_w d_w + \rho_m h) g \sin(\theta) - \rho_w d_w g \sin(\theta),$$

where ρ_m is the membrane's density. Consequently we find

$$a_n = \frac{(N-n)}{\eta_w}(\rho_w d_w + \rho_m h) g \sin(\theta) + \frac{f}{\eta_w}.$$

Besides, we also know that $\Delta u_n = \frac{t_2}{\mu}$, where μ is the two dimensional reduction of the viscosity coefficient μ_m, i.e, $\mu = \frac{\mu_m}{h}$, and t_2 is the stress applied on the bilayer (Fig.7) which is equal to $\tau_n - P\sin(\theta) = \tau_n - \rho_m h g \sin(\theta)$. This way we get

$$\Delta u_n = \frac{(N-n-1)}{\mu}(\rho_w d_w + \rho_m h) g \sin(\theta) + \frac{f}{\mu}.$$

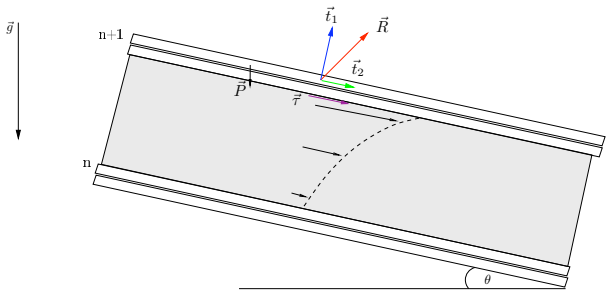

Figure 7: Representation of the forces that act on the layers. Here, $\vec{R}$ stands for the force induced by the layers above on the $n+1^{th}$ bilayer; $\vec{P}$ is the weight of a bilayer and $\vec{\tau}$ is the longitudinal component of the stress vector on the n^{th} water layer.

Inserting the last results into equation (1) we get

$$\begin{aligned} U_0 &= \sum_{n=1}^{N}\left[\frac{(N-n-1)}{\mu}(\rho_w d_w+\rho_m h)g\sin(\theta)+\frac{f}{\mu}\right]+ \\ &\quad +\sum_{n=1}^{N-1}\left[-\frac{\rho_w d_w^2}{2\eta_w}g\sin(\theta)+\frac{(N-n)}{\eta_w}(\rho_w d_w+\rho_m h)d_w+\frac{d_w}{\eta_w}f\right] \\ &\simeq \frac{N^2}{2}\left(\frac{1}{\mu}+\frac{d_w}{\eta_w}\right)(\rho_w d_w+\rho_m h)g\sin(\theta)+N\left(\frac{1}{\mu}+\frac{d_w}{\eta_w}\right)f \\ &= \left(\frac{1}{\mu}+\frac{d_w}{\eta_w}\right)\frac{L}{h+d_w}f+\left(\frac{1}{\mu}+\frac{d_w}{\eta_w}\right)(\rho_w d_w+\rho_m h)\frac{L^2}{2(h+d_w)^2}g\sin(\theta). \end{aligned}$$

In the last calculation we kept only the terms with higher order in N using the fact that $N \gg 1$ [2]. Moreover, if f is given by $M_A g\sin(\theta)$, where M_A is the lamelle's mass per unit area, we finally obtain the expression

$$\frac{U_0}{Lg\sin(\theta)}=\left(\frac{1}{\mu d_w}+\frac{1}{\eta_w}\right)\left(\frac{d_w M_A}{h+d_w}+(\rho_w d_w+\rho_m h)\frac{Ld_w}{2(h+d_w)^2}\right)\propto\frac{1}{\eta_{\text{effective}}}.$$

If we take the limits $\mu\to\infty$ and $h\to 0$, we find

$$U_0=\frac{1}{\eta_w}\left(M_A+\frac{L\rho_w}{2}\right)Lg\sin(\theta),$$

as we should get for a liquid without amphphilic bilayers.

The last expression can give us an idea of how the fluidity ($\frac{1}{\eta_{\text{effective}}}$) behaves with the membrane's inter-distance.

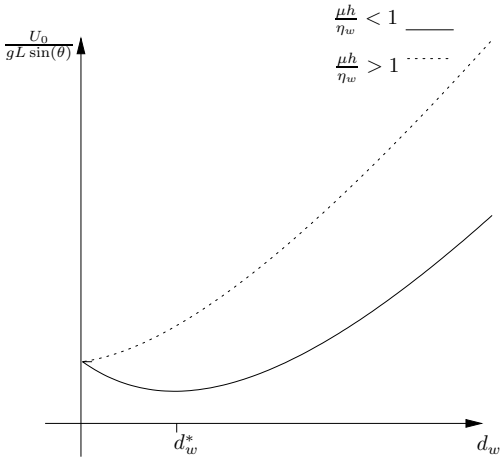

Figure 8: Fluidity ($\frac{1}{\eta_{effective}}$) versus d_w.

[2] In fact if we use a distance L of the order 100μm and bilayers with $h,\ d$ of the order 10nm we find that N is of the order 1×10^4 which ensures that assumption.

We observe two cases: if $\frac{\mu h}{\eta_w} \geq 1$ the effective viscosity decreases as d_w increases, but if $\frac{\mu h}{\eta_w} < 1$ it increases until it reaches a maximum at $d_w = d_w^*$ and then increases monotonically. For the first case we can estimate $\frac{U_0}{Lg\sin(\theta)}(d_w = 0)$ which corresponds to the maximum effective viscosity we can measure. We take $\rho_m \sim 10^3 \text{kg/m}^3$, $L \sim 1 \times 10^{-4}\text{m}$, $\mu h \sim 10^{-3}\text{kg/ms}$ and $M_A \sim 10^{-1}\text{kg/m}^2$, from which we get $\text{Min}(\frac{U_0}{Lg\sin(\theta)}) \sim 100\text{s/m}$.

1.3 Determination of the diffusion coefficient

The FRAPP technique, or fluorescence recovery after photobleaching in pattern, is a conventional method to study transport phenomena in biological membranes. It consists in photobleaching the transporters, fluorescent molecules, this means make them to lose fluorescence ability, and then following the recovery of fluorescence. As we will see, this recovery is related to the diffusion coefficient by means of an exponential decay which depends on the pattern fringe used.

We assume that the transporters have a brownian motion, this is

$$\frac{\partial}{\partial t}C(\vec{r},t) = D\nabla^2 C(\vec{r},t), \tag{2}$$

where $C(\vec{r},t)$ is the transporter distribution and D is the diffusion coefficient. After photobleaching the fluorescence intensity is done by

$$F(t>0) = \int C(\vec{r},t)I(\vec{r},t>0)d^3\vec{r}, \tag{3}$$

where $I(\vec{r},t>0)$ is the light's intensity which is much smaller than the photobleaching one. We assume an incident wave with intensity

$$I(\vec{r},t>0) = I_0\left(1+\cos(\vec{q}_0.\vec{r})\right). \tag{4}$$

Passing to Fourier space we have

$$F(t>0) = \int d^2\vec{q}\hat{C}(\vec{q},t)\hat{I}(-\vec{q},t>0), \tag{5}$$

assuming at this point two dimensional diffusion. Solving equation (2) in Fourier space we find

$$\hat{C}(\vec{q},t) = \hat{C}(\vec{q},0)\exp(-Dq^2t).$$

The Fourier transform of $I(\vec{r},t>0)$ is

$$\hat{I}(-\vec{q},t>0) = I_0\left(\delta(\vec{q}) + \frac{\delta(\vec{q}-\vec{q}_0)+\delta(\vec{q}+\vec{q}_0)}{2}\right).$$

Introducing these last results into expression (5) we get

$$F(t>0) = I_0\left(\hat{C}(0,0) + \frac{\hat{C}(\vec{q}_0,0)+\hat{C}(-\vec{q}_0,0)}{2}\exp(-Dq_0^2t)\right).$$

We see that independently of the initial distribution we will get an exponential decay which is simply related to the pattern fringe (Fig.9). However, the initial distribution will have an important

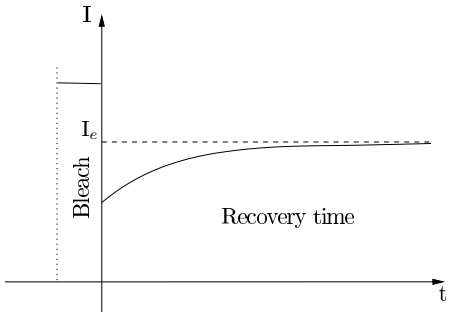

Figure 9: FRAPP recovery curve.

influence when trying to measure the exponential decay. To simplify the problem, we suppose that the bleaching pulse is composed of planar waves normal to the x axis. The light intensity is given by

$$I(\vec{r}) = I_b \left(1 + \cos(\vec{q_0}.\vec{r})\right).$$

Although it is difficult to predict the initial concentration profile, we can admit, if the bleaching time Δt is much shorter than the characteristic diffusion time, that the initial distribution is given by

$$\begin{aligned} C(\vec{r}, 0) &= C_0 \exp(-\alpha I(\vec{r})\Delta t) \\ &= C_0 \exp\left[-K\left(1 + \cos(\vec{q_0}.\vec{r})\right)\right], \end{aligned}$$

with $K = -\alpha I_b \Delta t$. We make a Fourier expansion

$$C(\vec{r}, 0) = C_0 \sum_{n=-\infty}^{\infty} A_n(K) \exp(in\vec{q_0}.\vec{r}).$$

The coefficients A_n are given by

$$A_n(K) = (-1)^n I_n(K) \exp(-K),$$

where $I_n(K)$ is a modified Bessel function. If we put these results into the expression (5) we find

$$F(t > 0) \simeq A_0(K) + A_1(K) \exp(-Dq_0^2 t) + \ldots + A_n(K) \exp(-Dn^2 q_0^2 t) + \ldots$$

The most important terms are given by $A_0(K)$ and $A_1(K)$. If we do a plot of the functions $I_0(K)$ and $I_1(K)$ we realize that for small K, that is, for weak bleaching efficiency, the amplitude A_1 can be much smaller than A_0, which difficults the measuring. We can solve this problem introducing a modulated phase with a frequency which is recovered after amplification. In this case we have

$$I(\vec{r}, t > 0) = I_0 \left(1 + \cos(\vec{q_0}.\vec{r} + \phi(t))\right),$$

with $\phi(t) = u \sin(\omega t)$. The expression for the fluorescence $F(t > 0)$ is periodic which allows us to take its Fourier transform

$$F(t > 0) = \sum_{n=0}^{n=-\infty} f_{2n}(t) \cos(2n\omega t),$$

where the coefficients $f_{2n}(t)$ are given by

$$\begin{aligned} f_0(t) &= I_0 \left(\hat{C}(0,0) + J_0(u)\hat{C}(\vec{q}_0,0)\exp(-Dq_0^2 t \right) \\ f_{2n}(t) &= 2I_0 J_{2n}(u)\hat{C}(\vec{q}_0,0)\exp(-Dq_0^2 t), \end{aligned}$$

where J_k is a Bessel function of order k. We choose u for which $J_2(u)$ is a maximum. The fact that we can only find frequencies multiples of 2ω, constitutes, in practice, a good way to control the quality of the measurements. The last results can be found in [4] and [2].

2 Experimental procedures

As we said earlier, our experience is divided in two parts. In the first we construct an experiment to measure the membrane's viscosity. If we have success we determine the diffusion coefficient using the FRAPP technique.

2.1 Determination of the membrane's viscosity

There are two important things we have to assure during the experience. First, the model we have assumed (Fig.6) requires that the amphiphilic membranes be parallel to the lamelle. Because this system is birefringent, if we use polarized light to illuminate it, we know that it will be well oriented if there won't be any light after it passes a transverse analyzer. The other resides on the fact that the solution contains hexanol which evaporates easily. Therefore we need to put the solution in a hermetically closed box.

In Fig.10 is shown the experimental apparatus. After recording the lamelle's movement with a webcam we have used a program called *Tracker*[3] to analyze the video and determine the velocity U_0.

Using the microscope's micrometer we can measure the thickness L by focusing on different plans. We used two methods (Fig.11). The first method presents less error sources. Contrary to the second, we don't need to know the refractive index of the solution, value we assumed to be approximately the water's index. Unfortunately it has disadvantages too. Because the solution has hexanol we can't use glue to fix the hole. Hence we used the method *a)* for the silicone, while for the amphiphilic solution we employed the second. For the first method the height L is given by

$$L = H - h$$

as can be easily seen in Fig.11a). For the second we used geometric optics to find

$$L = n_{\text{solut}} H - 2\frac{n_{\text{solut}}}{n_{\text{glass}}} h,$$

where n_{solut} is the refractive index of the solution. We experimented the two methods in the same liquid and the results matched quite well.

[3] *Tracker* is a video analysis package built on the *Open Source Physics Java Framework*. We can download it at http://www.cabrillo.edu/~dbrown/tracker/

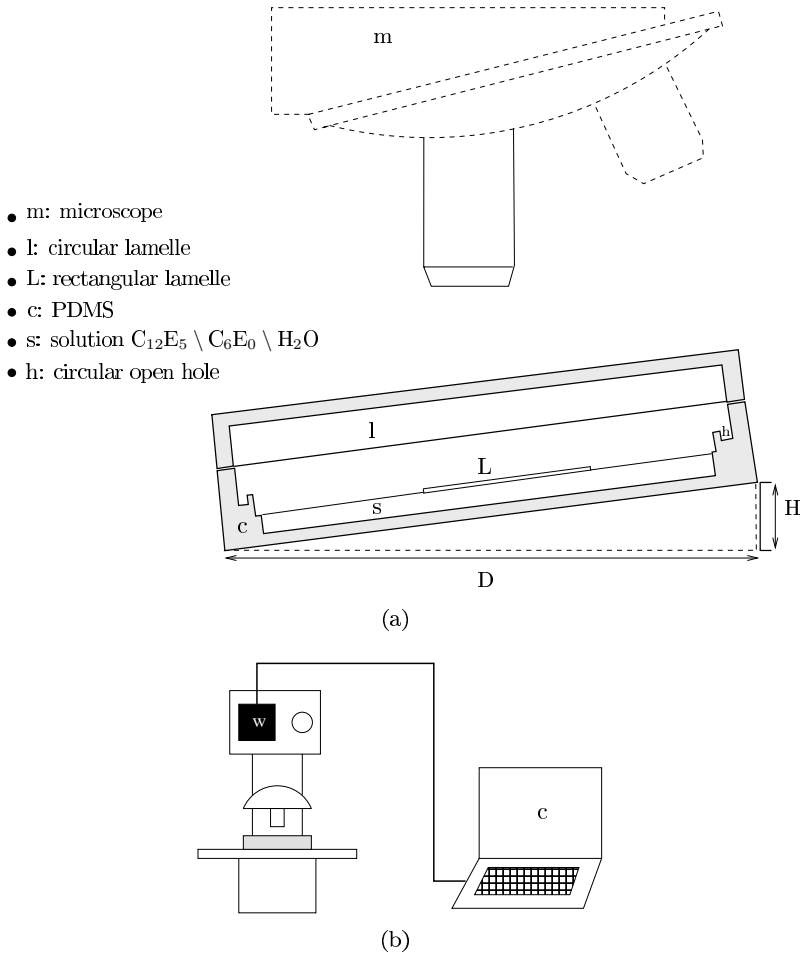

Figure 10: Experimental apparatus used for measuring the membrane's viscosity. a) detailed characterization of the liquid's box; b) general apparatus, c: laptop, w: webcam;

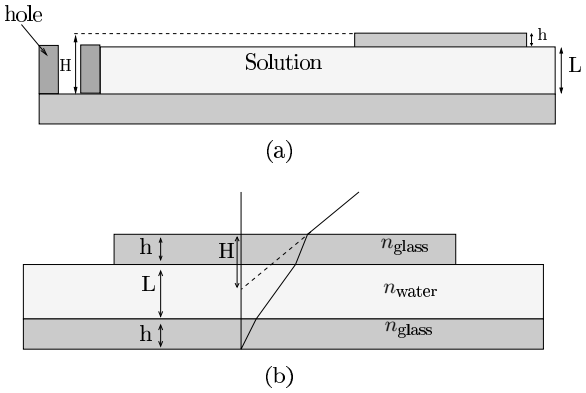

Figure 11: Methods used to determine the height L.

2.2 Preparation of the amphiphilic solution

We prepared solutions with different periods d, ranging from 40 to 200. Here is the formulae used to prepare the solutions,

$$\begin{aligned} \mathrm{V_{H_2O}} &= (1-\phi)100 \\ \mathrm{V_{C_{12}E_5}} &= 100\frac{\phi}{1+\rho_{\mathrm{v}}} \\ \mathrm{V_{C_6E_0}} &= \rho_{\mathrm{v}}\mathrm{V_{C_{12}E_5}}, \end{aligned}$$

where ρ_{v} is given by $\frac{d_{\mathrm{C_{12}E_5}}}{d_{\mathrm{C_6E_0}}}\rho_m$. The value for ρ_m was chosen to be 0,29 because it gives us a wide range of different distances d_w, as we see in Fig.5, and it was well studied in other works.

ϕ(%)	10	15	19	30	50
d(Å)	200	133	100	60	40
$C_{12}E_5$(%Vol)	7,5	11,2	14,2	22,4	37,3
C_6E_0(%Vol)	2,5	3,8	4,8	7,6	12,7
H_2O(%Vol)	90	85	81	70	50

Table 1: Prepared amphiphilic solutions.

2.3 Determination of the diffusion coefficient

In this experiment we use the same solutions we use to mesure the viscosity. In addition we put some fluorescent substances, known as markers, that will play the role of the MexB pump proteins. Using the FRAPP technique we can determine their diffusion coefficient.

In the Fig.12 is represented a schematic representation of the FRAPP experiment setup. The photobleaching period is characterized by a short intense incident light which is not modulated. After this period, the modulation unit is turned on and the intensity of the laser light is drastically reduced. This modulation, based on the action of a piezoelectric, induces an oscillating phase with frequency ω on the pattern fringe. The sample's fluorescence is then amplified by a photomultiplier and the second harmonic with frequency 2ω is then recovered by the lock-in amplifier.

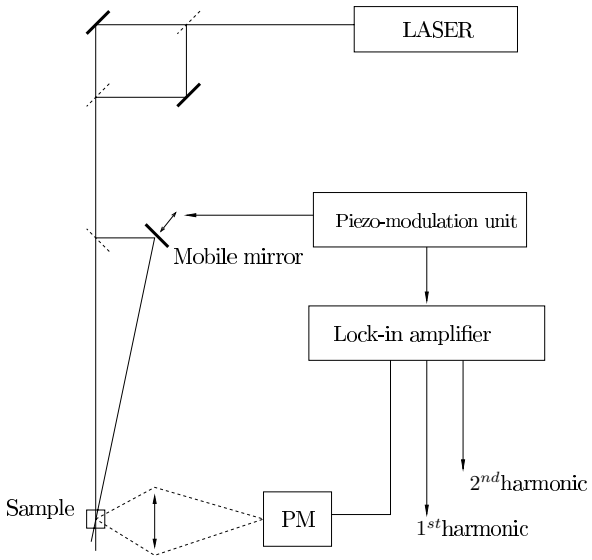

Figure 12: Schematical representation of the FRAPP setup. PM stands for photomultiplier.

3 Results

3.1 Viscosity

To have an idea of how accurate could be our measures, we did some tests using silicon oil. We tried three silicones of viscosities 100, 500 and 1000 cP (1 centipoise (cP)=10^{-3}Pa.s).

Using the Navier-Stokes equations we find

$$U_0 = \frac{1}{\eta} Lg(M_A + \frac{L\rho}{2}) \sin(\theta),$$

where ρ is the silicone's mass density and M_A is the lamelle's mass per unit area. Next we present the behavior of $Q = \frac{U_0}{Lg(m+\frac{L\rho}{2})}$ as function of $\sin(\theta)$ for the different oils.

The slope of the linear fit gives us $\frac{1}{\eta}$. This way we can determine the viscosity.

We begin with the silicone with higher viscosity, 1000 cP. The data is presented, first, in Tab.2 and then as a graph with the correspondent linear fit in Fig.13.

$\sin(\theta)$; $\Delta\sin(\theta)(\%)$=0,1	Q(m.s.kg^{-1})	ΔQ(%)
0,0056	0,0038	22
0,0111	0,0095	12
0,0167	0,0132	17
0,0222	0,0216	4
0,0278	0,0238	14
0,0334	0,0332	5
0,0445	0,0367	19

Table 2: Silicone 1000 cP; $M_A = 0,37 \pm 5\%\text{kg/m}^2$; $\rho = 0,82 \pm 1\%\text{kg/m}^3$

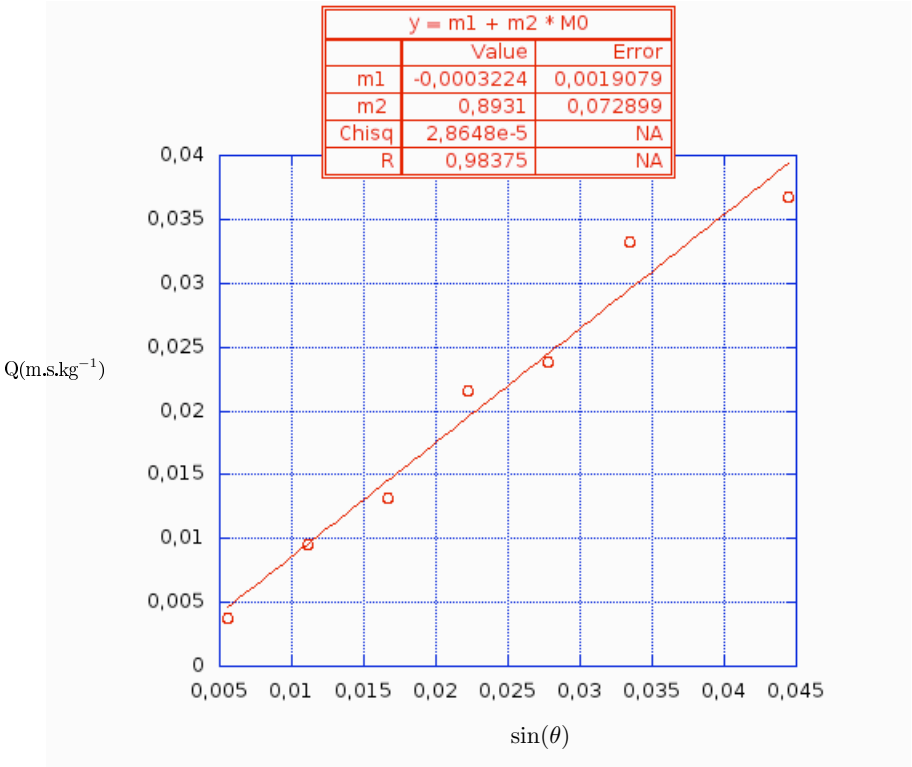

Figure 13: Silicone 1000 cP; Behaviour of Q as function of $\sin(\theta)$.

For this silicone we found a value of $1120 \pm 8\%$ cP for the viscosity which agrees very well with the expected value of 1000 cP. Moreover the fit passes very close to the origin as we expected theoretically.

The results concerning the silicone with expected viscosity of 500 cP are presented in Tab.3 and they are further plotted in Fig.14.

$\sin(\theta)$; $\Delta\sin(\theta)(\%)$=0,1	Q(m.s.kg^{-1})	ΔQ(%)
0,0167	0,0286	17
0,0345	0,0546	21
0,0500	0,094	8
0,0655	0,1057	25
0,0831	0,1412	17

Table 3: Silicone 500 cP; $M_A = 0,37 \pm 5\%\text{kg/m}^2$; $\rho = 0,82 \pm 1\%\text{kg/m}^3$

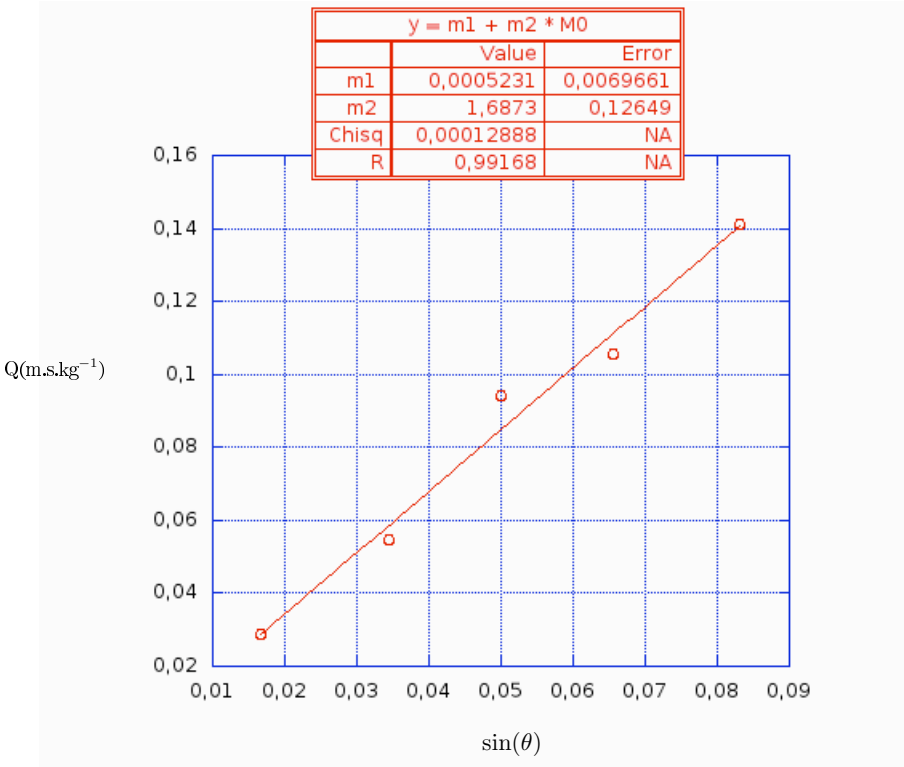

Figure 14: Silicone 500 cP. Behaviour of Q as function of $\sin(\theta)$.

This time we get $593 \pm 7\%$ cP for the viscosity. It is 19% far from the expected 500 cP. We also get a value for the velocity at angle $\theta = 0$ very close to zero.

Next we present the results of the last silicone oil with 100 cP of expected viscosity.

$\sin(\theta)$; $\Delta\sin(\theta)(\%)$=0,1	Q(m.s.kg^{-1})	ΔQ(%)
0,0111	0,0121	12
0,0167	0,0396	10
0,0222	0,5900	11
0,0334	0,1068	25
0,0445	0,1359	20
0,0556	0,2190	15
0,0667	0,2622	20

Table 4: Silicone 100 cP; $M_A = 0,37 \pm 5\%\text{kg/m}^2$; $\rho = 0,82 \pm 1\%\text{kg/m}^3$

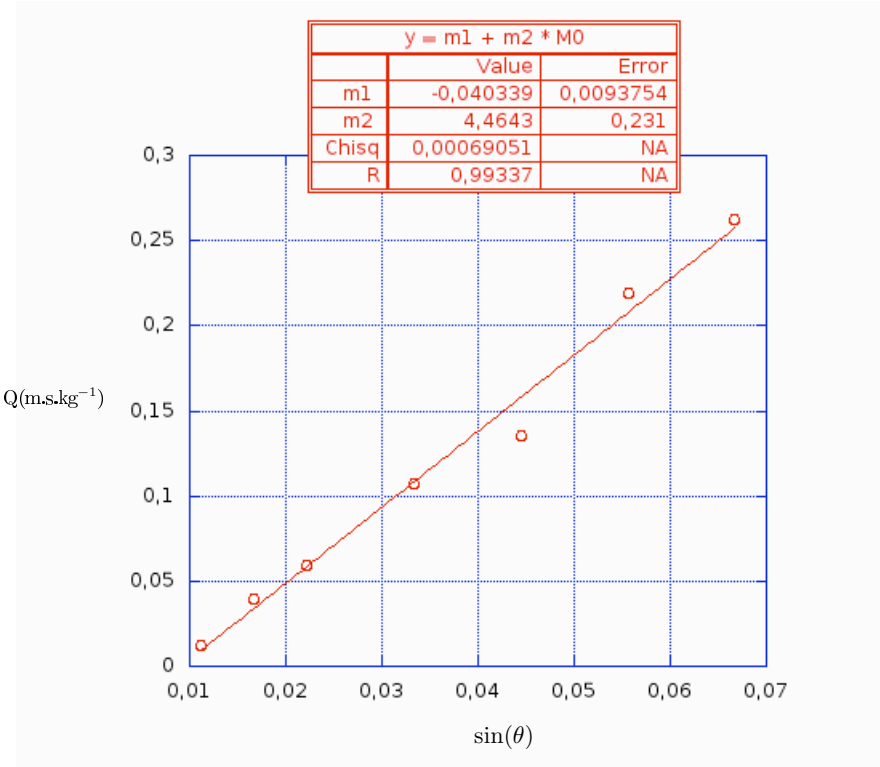

Figure 15: Silicone 100 cP. Behaviour of Q as function of $\sin(\theta)$.

The fit gives us $224 \pm 5\%$ cP for the viscosity. It constitutes a 55% deviation from the expected value 100 cP.

The last results are resumed in Tab.5. They present almost the same accuracy but as long as we mesure less viscous oils we get higher deviations. Nevertheless this range of viscosities $100-1000$ cP is a good depart for the next experiences.

Next we present the results concerning the experiment with the amphiphilic solution. The solutions with $\phi = 0,3/0,5$ showed a relatively high viscosity. We found that the orientation of the

η_{expected}(cP)	$\eta_{\text{exp.}}$ (cP)	Deviation(%)=$\frac{\lvert\eta_{\text{expected}}-\eta_{\text{experi.}}\rvert}{\eta_{\text{expected}}}$	Precision error (%)
100	224	55	5
500	593	19	7
1000	1120	12	8

Table 5: Experimental values for the silicone's viscosity.

amphiphilic bilayers was more difficult for higher viscosities, which avoided their study. We also found that the movement of the lamelle was not uniform showing a small deceleration in contrast to the silicone case where it was uniform. As a consequence we tried to collect the movement's data as quick as possible.

We present in Tab.6 the experimental values of U_0 as function of $\sin(\theta)$ for an amphiphilic solution with $\phi = 0,19$. They are further plotted with the associated linear fit (Fig.16).

$\phi = 0,19$	$d = 100$Å	$L_{\text{med}} = 280 \pm 5\mu$m
$\sin(\theta)$	U_0=Vmed(μm/s)	Error(%)
0,011	2,1	14
0,022	6,7	28
0,033	12,2	18
0,045	20,9	50
0,056	35,9	8*

Table 6: Amphiphilic solution with $\phi = 0,19$. The point marked with the * was not considered because it was far from the linear fit.

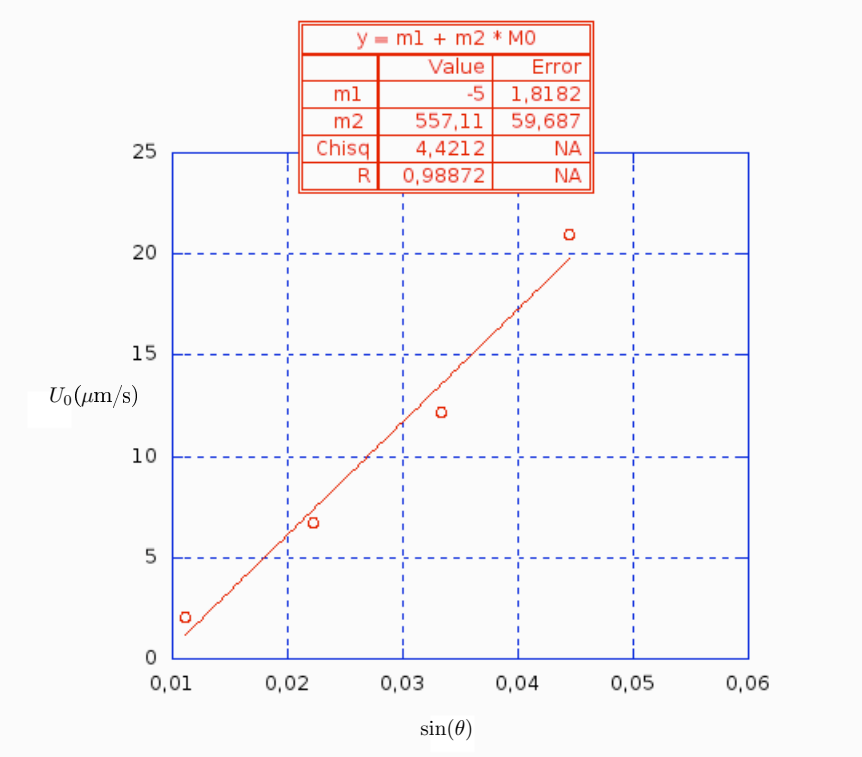

Figure 16: Amphiphilic solution with $\phi = 0,19$; Behaviour of the velocity U_0 as function of $\sin(\theta)$.

We find an effective viscosity ($\eta_{\text{effec}} = \frac{M_A L g \sin(\theta)}{U_0(\theta)}$) of $1850 \pm 17\%$ cP.

In Tab.7 is presented the data for the amphiphilic solution with $\phi = 0,15$. It is further plotted with the correspondent linear fit (Fig.17).

$\phi = 0,15$	$d = 133$Å	$L_{\text{med}} = 34 \pm 5\mu$m
$\sin(\theta)$	U_0=Vmed(μm/s)	Error(%)
0,0111	4,2	8
0,0167	10,1	10
0,0222	14,2	10
0,0278	20,0	29

Table 7: Amphiphilic solution with $\phi = 0,15$.

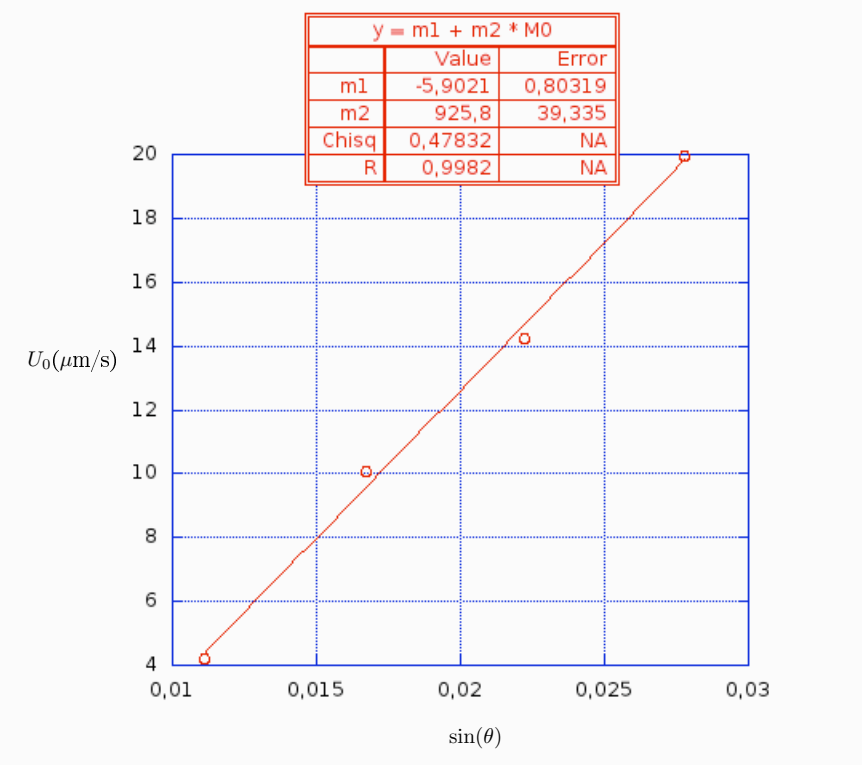

Figure 17: Amphiphilic solution with $\phi = 0,15$. Behaviour of the velocity U_0 as function of $\sin(\theta)$.

This time we get $\eta_{\text{effect}} = 134 \pm 25\%$ cP.

Finally, in Tab.8 we show the results for the solution with $\phi = 0,10$. In Fig.18 is represented a plot with a linear fit.

$\phi = 0,10$	$d = 200$Å	$L_{\text{med}} = 52 \pm 5\mu$m
$\sin(\theta)$	Vmed(μm/s)	Error(%)
0,0056	1,6	38
0,0111	15,6	11
0,0145	15,8	9
0,0167	23,8	23

Table 8: Amphiphilic solution with $\phi = 0,10$.

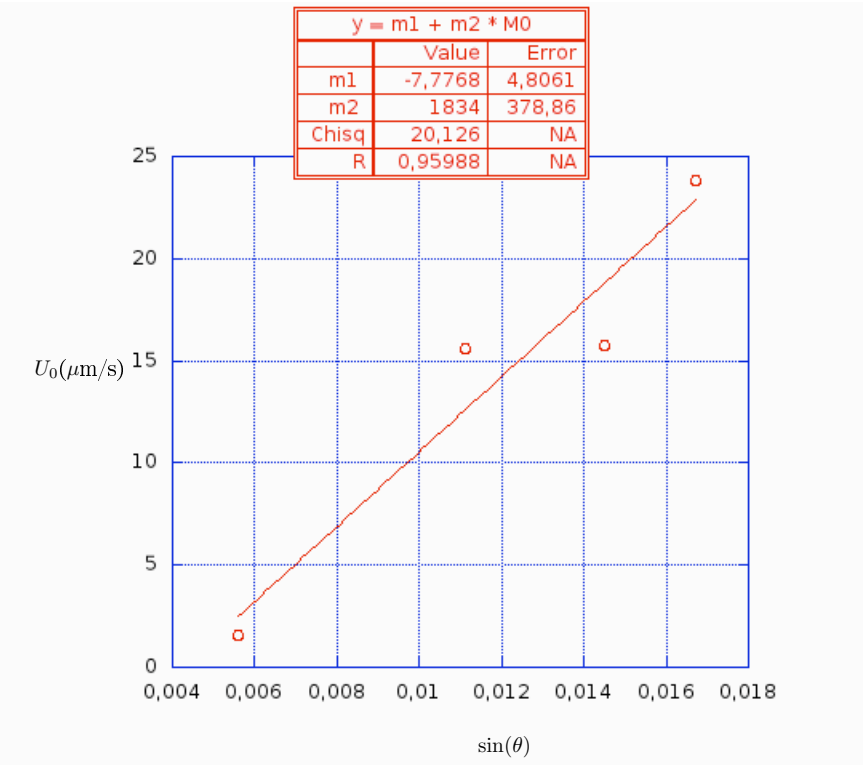

Figure 18: Amphiphilic solution with $\phi = 0,10$. Behaviour of the velocity U_0 as function of $\sin(\theta)$.

For this solution we obtained $\eta_{\text{effect}} = 103 \pm 35\%$ cP.

The graphs show us that all the linear fits pass far from the origin although they present good regression coefficients (R). In Tab.9 we express the behavior of the fluidity $\frac{U_0}{Lg\sin(\theta)}$ and the effective viscosity for the different solutions. From it we see that the results are less precise for smaller viscosities in contrast to the silicone experiment where they were smaller and homogeneous. Moreover, the values for $\frac{U_0}{Lg\sin(\theta)}$ are much smaller from those we expected which were of the order 100s/m. This gives us negative values for the membrane's viscosity and the associated errors are very small to cover positive values (Tab.10).

ϕ	d(Å)	$F = \frac{U_0}{Lg\sin(\theta)}$(s/m)	ΔF(%)	η_{effect}(cP)	$\Delta\eta$(%)
0,19	100	0,20	12	1850	17
0,15	133	2,77	19	134	25
0,10	200	3,60	30	103	35

Table 9: Fluidity versus ϕ.

ϕ	d_w(Å)	$\mu d_w(10^{-3}$Pa.s)	$\Delta(\mu d_w)$
0,19	100	-1,001	$0{,}06*(\mu d_w)^2$
0,15	133	-1,009	$1{,}6*(\mu d_w)^2$
0,10	200	-1,010	$3{,}03*(\mu d_w)^2$

Table 10: Membrane's viscosity for different periods d.

3.2 Diffusion coefficient

Unfortunately we couldn't determine the diffusion coefficient. The solutions on the capillaries took too much time to get oriented. The FRAPP didn't show any diffusion in the oriented regions. We think that the fluorescent markers concentrated in non-oriented regions as a consequence of the long waiting time.

4 Discussion & conclusion

The first experiences with the silicone show us that we can measure viscosities with a reasonable accuracy. We get better results for higher viscosities, as we can easily verify in Tab.5. For example, for the silicone 1000 cP we get a deviation of 12% which constitutes a pretty result if we get into account the limitations of the experience. In fact, we know theoretically that for lower Reynolds numbers the laminar flow is easily achieved, that is, the border effects are less important and the inertial forces are negligible.

Regarding the amphiphilic solutions we find relatively different results. We see from the graphs that the linear fits aren't as good as the silicone ones. On the contrary to the silicone, we find that the velocity at the origin is not zero as we would expect. Moreover, we found that the movement of the lamelle was not uniform presenting a small deceleration. Although we couldn't find an explanation for the deceleration, we think that it was due to the fact that the liquid height was not constant during the experiment. Most important is the fact that we find fluidities that are much smaller (a factor of the order 100) than those we could expect theoretically (sec.1.2). As presented in Tab.10 the values for μ are negative and its error is to small to cover positive values. The errors commited are too small, the order of 20%, to explain the discrepancy. Besides, the solution was well oriented during the experience which make us believe in the model proposed above, that is, of a periodic system of parallel amphiphilic bilayers. Probably the discrepancy is related to the fact that the movement was not uniform.

In conclusion, we can say that this experience as it is constructed is not suitable to study the membrane's viscosity. Although we obtained good results in determining the silicone's viscosity we found for the membranes values that doesn't match theoretically.

References

[1] Vincent Cattoir. Pompes d'efflux et resistance aux antibiotiques chez les bacteries, efflux-mediated antibiotics resistance in bacteria. *Elsevier PATBIO*, 2004.

[2] Didier Chatenay. *Diffusion, solubilisation et phenomenes interfaciaux dans les solutions isotropes d'amphiphiles.* PhD thesis, Ecole Normal Superieure de Paris, 1987.

[3] Jacob N. Israelachvili. *Intermolecular and surface forces.* Academic Press, 1991.

[4] Philippe F.Devaux Jean Davoust and Liliane Leger. Fringe pattern photobleaching, a new method for the measurement of transport coefficients of biological macromolecules. *EMBO*, 1982.

[5] Amir Maldonado. *Structure et topologie de phases fluides de bicouches. Mesures d'autodifusion de marqueurs et de diffraction de rayons X.* PhD thesis, Universite Paris 6.

[6] Patrick Moreau. *Diffusion moleculaire d'un dopant hydrosoluble dans une phase lamellaire lyotrope; Transition smectique-cholesterique dans un melange de molecules amphiphiles.* PhD thesis, Universite Bordeaux I, 2004.

[7] P. G. Saffman and M. Delbruck. Brownian motion in biological membranes. *PNAS*, 1975.

[8] M. Reffay E. Sierecki N. S. Gov M. Genest R. S. Hodges Y. Gambin, R. Lopez-Esparza and W. Urbach. Lateral mobility of proteines in liquid membranes revisited. *PNAS*, 2006.